Stimulus Responsive 3D Assembly for Spatially Resolved Bifunctional Sensors

Cheng Zhang, Heng Deng, Yunchao Xie, Chi Zhang, Jheng-Wun Su, and Jian Lin*

C. Zhang, H. Deng, Y. Xie, C. Zhang, J. W. Su, Prof. J. Lin

Department of Mechanical and Aerospace Engineering,

University of Missouri, Columbia, Missouri 65211, United States

Prof. J. Lin

Department of Electrical Engineering and Computer Science,

Department of Physics and Astronomy,

University of Missouri, Columbia, Missouri 65211, United States

*E-mail: LinJian@missouri.edu

Keywords: 3D structures, assembly, responsive, sensors, laser induced graphene

ABSTRACT

Three-dimensional (3D) electronic/optoelectronic devices have shown great potentials for various

applications due to their unique properties inherited not only from functional materials but also

from 3D architectures. Although a variety of fabrication methods including mechanically guided

assembly have been reported, the resulting 3D devices show no stimuli-responsive functions or

are not free standing, thereby limiting their applications. Herein, we demonstrate stimulus

responsive assembly of complex 3D structures driven by temperature-responsive hydrogels for

applications in 3D multifunctional sensors. The assembly driving force, compressive buckling,

arises from the volume shrinkage of the responsive hydrogel substrates when they are heated above

the lower critical solution temperature (LCST). Driven by the compressive buckling force, the 2D-

formed membrane materials, which are pre-defined and selectively bonded to the substrates, are

then assembled to 3D structures. They include "tent", "tower", "two-floor pavilion", "dome",

"basket", and "nested-cages" with delicate geometries. Moreover, the demonstrated 3D

bifunctional sensors based on laser induced graphene (LIG) show capability of spatially resolved

tactile sensing and temperature sensing. These multifunctional 3D sensors would open new

applications in soft robotics, bioelectronics, microelectromechanical systems (MEMS) and others.

1

1. INTRODUCTION

Electronics/optoelectronics in three-dimensional (3D) architectures have been broadly applied in biomedicine, [1-3] microelectromechanical systems (MEMS), [4-5] near-field communication (NFC), [6] and imaging, [7] because of their astounding properties such as high integration density, fast operation speed, high specific area, and multifunctionalities, compared to the traditional twodimensional (2D) counterparts. [8-11] 3D electronics are first realized via stacking multilayer 2D devices. [12] which is a straight forward route derived from advanced microfabrication technologies. To make the stacked layers work in synergy, however, complicated interconnects for electrical or/and optical connection among these layers are required. [13] Besides, the structures of the stacked 3D electronics are highly bulky, [14] thus does not fully utilize advantage of the high specific area of the 3D structures. In contrast, 3D printing technique provides structural versatility for fabricating 3D electronics. [15-18] For example, a bionic ear with a complex anatomic geometry has been fabricated via 3D printing of a cell-seeded hydrogel together with an intertwined conducting polymer.^[19] Nevertheless, 3D printing requires either the printing materials to be prepared as inks or to be sensitive to light, thus having limited or no access to advanced materials in different forms.[20-21]

An alternative approach, the stress-driven assembly, is fortunately accessible to various materials and capable of generating 3D heterogeneous electronic systems from prefabricated membrane-like materials.^[16, 18] Moreover, 3D devices can adapt to the working environment by post-fabrication assembly after delivered. For instance, implantable bioelectronics were designed to deploy to 3D structures from planar layouts when implanted into a physiological environment, thereby facilitating formation of conformal interfaces between the bioelectronics and the tissue.^[22] However, the traditional stress-driven assembly methods can only generate simple 3D

architectures from bending or folding of 2D precursors.^[16] In addition, the shapes of the assembled structures are irreversible.^[23] A new mechanically guided assembly based on compressive buckling has been demonstrated to yield complex and reversible 3D structures.^[16,20] Although this method has led to some 3D electronics including NFC devices,^[6] photodetectors^[7], antennas,^[24] and supercapacitors,^[25] their applications are highly restrained because these 3D devices have to be tethered on the cumbersome elastomeric substrates in order to maintain the 3D geometries, and the reversible assembly processes require bulky and complicated actuation apparatus.^[26]

To address aforementioned problems, our group has developed a responsive buckling induced assembly methodology.^[27] We replaced the cumbersome elastomeric substrates with responsive polymeric substrates^[28-30] whose shapes were transformed when they were exposed to external stimuli. The bending and folding of the responsive polymeric substrates imparted compressive stresses to the bonded 2D precursors, which actuated the 3D assembly. The assembly was reversible without manual intervention and the final 3D structures were free standing via the inclusion of the responsive polymeric substrates as parts of the final architectures. This strategy has been applied to assemble a light-emitting diode (LED) and a 3D flex sensor.^[27] However, the stimulus of acetone is toxic, which limits its practical applications. In addition, as they only involved bending and folding actuation, relatively simple 3D structures were realized.

Herein, we demonstrate a stimulus responsive assembly of 3D electronic sensors actuated by a hydrogel which is responsive to a moderate temperature (~35 °C). Briefly, 2D precursors and the thermo-responsive polymer hydrogel, poly(N-isopropylacrylamide) (PNIPAM),^[31] were first cut with designed layouts by a mask-free direct laser writing (DLW)^[32-33] fabrication technique (Figure 1a). Afterwards, the 2D precursors were selectively bonded onto the hydrogel substrates. When the applied temperature was above the lower critical solution temperature (LCST),^[34] the

hydrogel substrates shrank and imparted compressive buckling forces to the bonded 2D precursors for the 3D assembly (Figure 1b). When the temperature was below LCST, the hydrogel substrates had water uptake to expand their volume to original one, thus making the 3D structures recover to 2D sheets. By this way, various 3D structures including "tent", "tower", "two-floor pavilion", "dome", "basket", and "nested-cages" were assembled from the SU-8 and polyimide (PI) films, which are commonly used supporting layers for flexible electronics.^[35] Then a 3D bifunctional sensing system, whose sensing element was made from laser induced graphene (LIG). [36-37] was fabricated by the stimulus responsive assembly of a planar strain sensor array and a temperature sensor array. Benefiting from the 3D configuration, this bifunctional sensor showed the capability of omnidirectional tactile sensing and spatially resolved temperature sensing. To the best of our knowledge, this is the first work that reports spatially resolved 3D sensors based on the responsive 3D assembly. The spatially resolved sensing function would lead to widespread potential applications. For instance, the omnidirectional tactile sensor applied in the robots would help to better identify the geometry of the contact objects. [38-39] The spatial temperature sensing function would enable to locate the heat source.

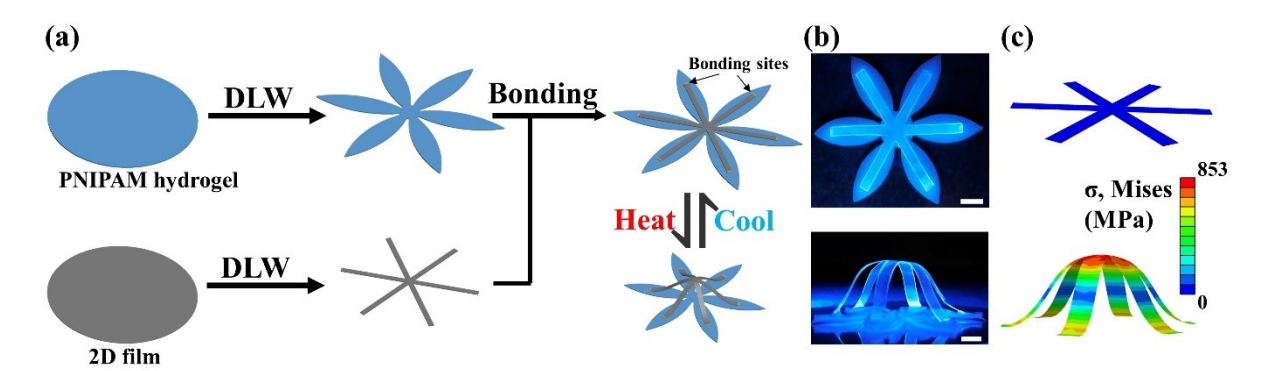


Figure 1. (a) Schematic of reversible self-assembly of 3D structures from 2D-formed materials selectively bonded onto PNIPAM hydrogel substrates. Photographs (b) and FEA modeling results (c) of a 3D structure assembled from a 2D SU-8 precursor. Scale bars: 5 mm.

2. RESULTS AND DISCUSSION

2.1 Temperature Responsive PNIPAM Hydrogel. Two properties were considered when a thermo-responsive hydrogel was selected: moderate responsive temperature that is compatible with device working conditions (< 70 °C)^[40] and a large volume shrinkage to provide sufficient compressive buckling force for driving the 3D assembly. The PNIPAM hydrogel is a promising candidate. Its LCST can be tuned to as low as 33 °C.^[34] Below LCST, the polymer chains of PNIPAM are coil (swollen state), tending to absorb water. Above LCST, the polymer chains of PNIPAM are globule (shrunk state), tending to expel water.^[31, 34] The transition from the swollen state to the shrunk state results in a large volume shrinkage of 38.5%.^[41]

We synthesized the PNIPAM hydrogel according to the reported recipe (see Experimental Section for details). [41] The thermal property of the hydrogel was characterized by the differential scanning calorimetry (DSC) (Figure S1). The spectrum shows that the onset point of the endothermic peak, which is defined as LCST, [42] is ~35 °C. Then a PNIPAM hydrogel with an initial diameter (D) of 3.5 cm was heated to 50 °C. As the temperature increased, the hydrogel expelled water and the ultimate diameter (d) shrank to 2.2 cm (Figure S2). It showed a linear shrinkage strain (ϵ_s) of 37% as calculated by $\epsilon_s = (D-d)/D \times 100\%$.

2.2 Responsive 3D Assembly. The 3D assembly driven by the shrinking of the PNIPAM hydrogel is illustrated in Figure 1a. The synthesized hydrogel was first cut to a designed pattern (e.g., "six-petal") by DLW. This pre-defined hydrogel would become a part of the final 3D structure, thus enhancing the structural complexity for practical applications.^[27] Similarly, a 2D precursor was shaped to a desirable pattern. For example, a SU-8 film with thickness of 35 μm

was cut into an "umbrella-rib" pattern. Then, a cyanoacrylate adhesive (Loctite 406, Henkel), which provided instant bonding between the hydrogels and various materials, [43] was placed on the designated spots of the patterned SU-8 film. Immediately, the SU-8 film was transferred and aligned onto the PNIPAM hydrogel substrate at room temperature. In just a few seconds, the cyanoacrylate adhesive was cured and selectively bonded the SU-8 film to the PNIPAM hydrogel substrate.

After the bonded SU-8/PNIPAM sample was heated to 50 °C (above LCST), the PNIPAM polymer chains expelled water and made the hydrogel substrate shrink. The shrinkage of the hydrogel compressed the SU-8 film through the bonding sites. As a result, the SU-8 planar film was assembled to a 3D "tent" structure. When the system was cooled down to room temperature, the PNIPAM hydrogel substrate reabsorbed water and expanded to its original volume, making the 3D SU-8 structure recover to the 2D sheet. This reversible shape transformation is shown in Figure 1b. The assembled structures were predicted and analyzed by finite element analysis (FEA), showing reasonable agreement with the experimental results (Figure 1c). Moreover, the stress distribution indicates that the maximal stress exists on the roof of the "tent". This information can help us to optimize the design in order to prevent structural failure due to the stress concentration. For example, the addition of the origami design on the stress concentration regions is able to alleviate the problem.^[44]

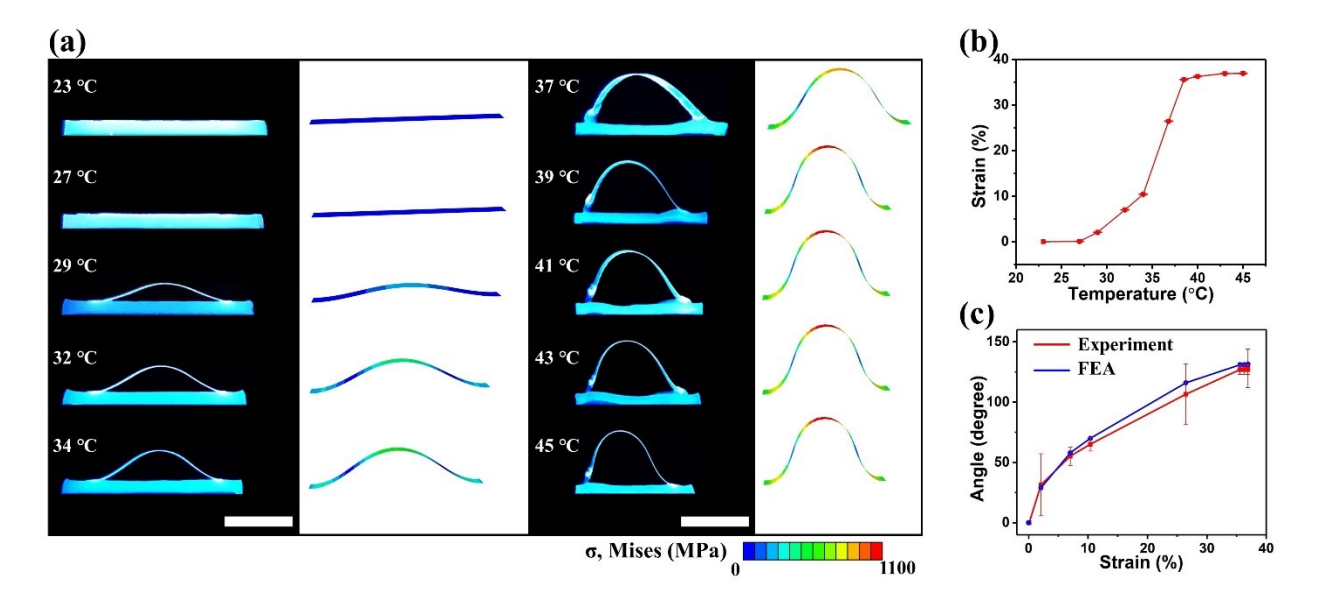


Figure 2. (a) Photographs and FEA results of a representative group of assembled structures from a ribbon model as temperature increases. Scale bars: 5 mm. (b) Relationship of linear shrinkage strains of PNIPAM hydrogel and stimulating temperatures. (c) Relationship of curving angles of SU-8 ribbons and linear shrinkage strains.

2.3 3D Structural Control. To better understand the assembly behaviors, we first tried to correlate temperature, shrinkage, and curving angle. The curving angle is defined as the angle between the two tangents near the peak [27, 44] as shown in Figure S3. The temperature induces the shrinkage (quantified by the linear shrinkage strain) of the PNIPAM hydrogel, and the shrinkage imparts compressive stress to the 2D film to form 3D structures (quantified by the curving angle). To achieve the goal, a structure schematically represented in Figure S3 was fabricated by bonding a SU-8 ribbon (15 mm \times 1 mm \times 0.035 mm) on selective sites of a PNIPAM hydrogel sheet (15 mm \times 3 mm \times 1 mm). Upon thermal stimulation, the SU-8 ribbon was buckled to an arc structure. As the temperature increases, the curving angle increases due to the enhanced linear shrinkage strains of the hydrogel substrate (Figure 2a). The curve showing relationship of the linear shrinkage

strain and temperature is plotted in Figure 2b. As the temperature rises from 20 °C to 27 °C, no volume shrinkage is noticed. The strain slightly increases to 2.08% when the temperature is 29 °C, and then linearly increases to 10.38% as the temperature increases to 34.5 °C. A significant leap to ~37% happens between 34.5 °C and 38.5 °C. This sharp transition at ~34.5 °C indicates that the phase change happens at LCST, agreeing well with the DSC result (LCST = 35 °C). Figure 2c reveals the relationship between the curving angle and the shrinkage strain. Overall, the angle increases from 0 degree to 127 degree as the shrinkage strain increases to 37%. FEA simulation well predicts their relationship, showing good agreement with the experimental results (Figure 2a and Figure 2c).

2.4 Assembly of Complex 3D Structures. The quantitative investigation indicates that the assembly process can be finely controlled by the temperature through regulating the shrinkage strain. With this guidance, more sophisticated 3D structures have been assembled from 2D precursors with varied patterns bonded to the hydrogel substrates. Figure 3a-c present representative 3D structures assembled from SU-8 films. In Figure 3a, a SU-8 film with a kirigami pattern of "six-arrow" was selectively bonded to a PNIPAM hydrogel substrate with a layout of "six-petal". When the hydrogel was heated to 37 °C, ~26.5% shrinkage strain was generated as expected, resulting in the assembly of a "tower" structure. More complex 3D structures were achieved by adding more layers of the 2D precursors. For example, a small (with diameter of 20 mm) and a large (with diameter of 30 mm) "umbrella-rib" SU-8 films were successively bonded to a "six-petal" hydrogel substrate (Figure 3b). After heated to 50 °C which resulted in 37% shrinkage strain, a "two-floor pavilion" 3D structure was assembled. Programming of the hydrogel substrates also improves the complexity of the assembled 3D structures. As shown in Figure 3c, a

3D "dome" architecture was assembled from a 2D "twelve-arrow" SU-8 film that was bonded onto a "twelve-petal" PNIPAM substrate at 50 °C. The sphericity of this 3D "dome" structure is much larger than that of the one shown in Figure 1, which can be attributed to the increased number of petals in the hydrogel substrate.

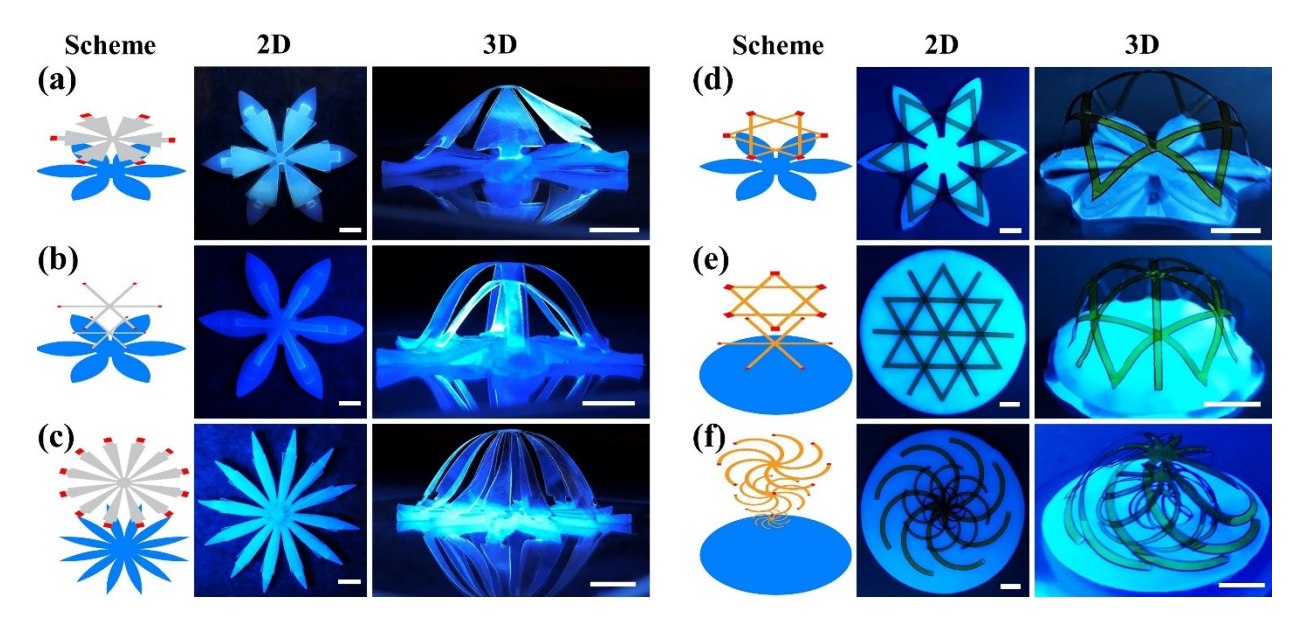


Figure 3. Schematics and photographs of 3D architectures assembled from SU-8 films (a–c) and PI films (d–f). Scale bars: 5 mm. In the schematics, blue, red, grey, and orange areas represent PNIPAM hydrogels, bonding sites, 2D SU-8 films, and 2D PI films, respectively.

This assembly can be easily applied to other materials, for example, polyimide (PI). To assemble the PI films with thicknesses of 25 µm, the PNIPAM hydrogel substrates were all heated to 50 °C to generate 37% shrinkage strain. First, a 3D "tent" structure was assembled from an "umbrellarib" PI film that was bonded to a "six-petal" PNIPAM substrate (Figure S4 and Movie S1). Figure 3d shows a 3D "open basket" structure assembled from a 2D "hexagram" PI film. More complex 3D structures were assembled from multilayered 2D precursors. For example, combination of an "umbrella-rib" and a "hexagram" resulted in a "close basket" when it was thermally stimulated

(Figure 3e). Furthermore, a 3D trilayer "nested-cage" structure was assembled from three PI films made of "windmill" patterns (Figure 3f). Besides the polymeric materials including SU-8 and PI films, this assembly method can be applied to other materials such as semiconductors and metals to fabricate 3D structures from 2D counterparts. [45] As demonstrated in Figure S5, a 3D "tent" structure was assembled from a 2D aluminum foil with thickness of 16 μm.

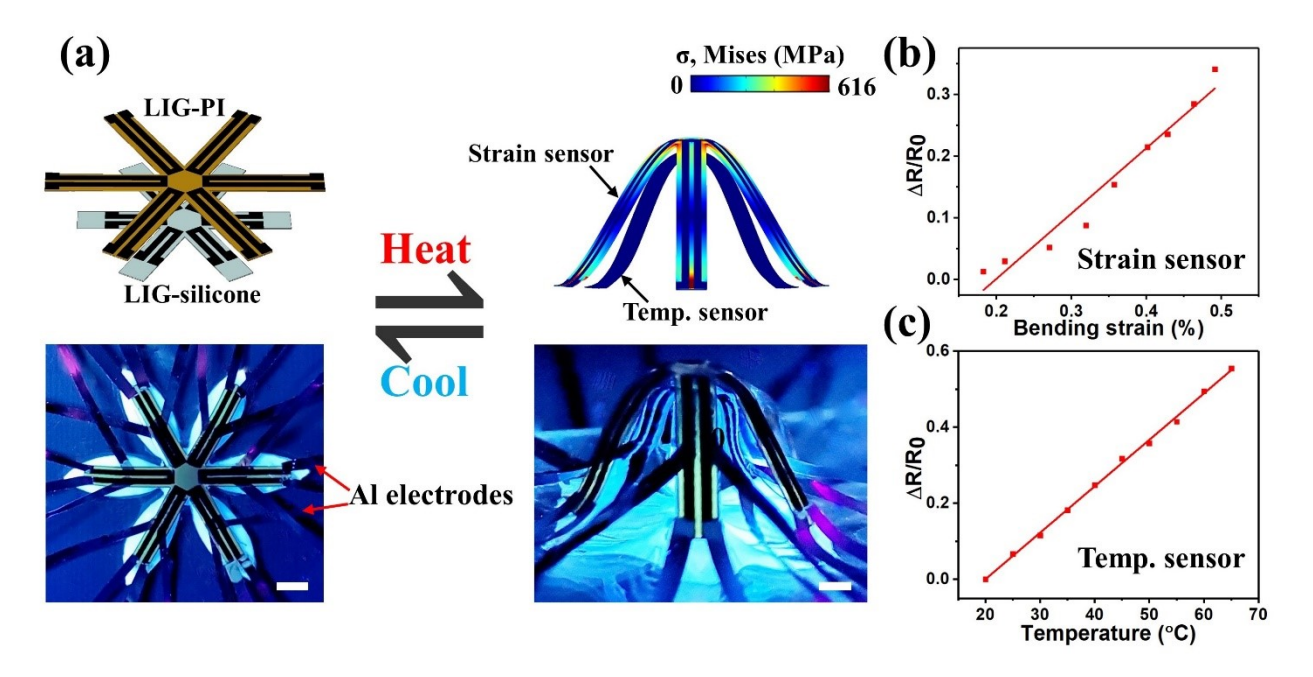


Figure 4. (a) FEA and optical images of 3D LIG bifunctional sensors consisting of a 3D strain sensor array and a 3D temperature sensor array. Scale bars: 5 mm. (b) Ratio of resistance change vs. bending strain in a LIG 3D strain sensor. (b) Ratio of resistance change vs. temperature in a LIG 3D temperature sensor.

2.5 3D Bifunctional Sensors. The demonstration based on the SU-8 and PI films has validated the feasibility of the proposed 3D assembly method. To demonstrate a practical application, we report a 3D bifunctional structure by the assembly of a 6-strain sensor array and a 6-temperature sensor array based on laser induced graphene (LIG)^[36-37] which was fabricated by DLW (Figure

4a). The LIG served as the sensing material. The detailed layouts for both sensor arrays are presented in Figure S6. When the LIG-PI sensors were bent, the generated strain in the LIG (Figure S7) leaded to misalignment of the conductive network, thus increasing its electrical resistance. [46] The curve of resistance change ratio ($\Delta R/R_0$, where ΔR is increased electrical resistance and R_0 is the original resistance) vs. bending strain is plotted in Figure 4b. It shows quite linear relationship. The temperature sensors were fabricated by transferring the LIG from the PI films to silicone substrates. The temperature sensing characteristic is shown in Figure 4c. When the LIG-silicone sensors were heated from 20 °C to 65 °C, the resistance change increased linearly by 58%, which can be attributed to the different thermal expansion coefficients of LIG and silicone. [33, 47]

What is more, the assembled 3D sensor shows functions of omnidirectional tactile sensing and spatially resolved temperature sensing. As shown in Figure 5a, when a strain sensor (Strain-1) was touched by an incoming force, its resistance was rapidly increased by 6%. As the touch was held, the resistance change maintained with a little attenuation. After the touch was removed, the resistance quickly dropped back to the initial value. If Strain-1 was fast clicked, the resistance showed a sharp increase ($\Delta R/R_0 = 7.2\%$) and then a sharp decrease to the initial value, which was different from the "hold" mode signal. By this way, the strain sensor can identify different modes of touch. The assembled 3D strain sensor array also showed the potential in omnidirectional tactile sensing. All six strain sensors can individually sense the strains induced by touch from their facing directions (Figure 5b and Figure S8). Therefore, the tactile signal from these six directions can be simultaneously detected. If the device density of the sensor array increases, we anticipate that this 3D sensing system can detect the strain with high spatial resolution. This demonstration would open new applications in robotics. Besides the strain sensing, the LIG-PI sensors can also sense forces. The resistance change ratio ($\Delta R/R_0$) increases with the applied force (Figure S9). When a

6.5 mN force was applied to the individual sensor, $\Delta R/R0$ showed abrupt increase (Figure S10), agreeing well with the result shown in Figure S9. After removing the force, the resistances recovered to the original values. Moreover, their sensing performance was repeatable (Figure S10).

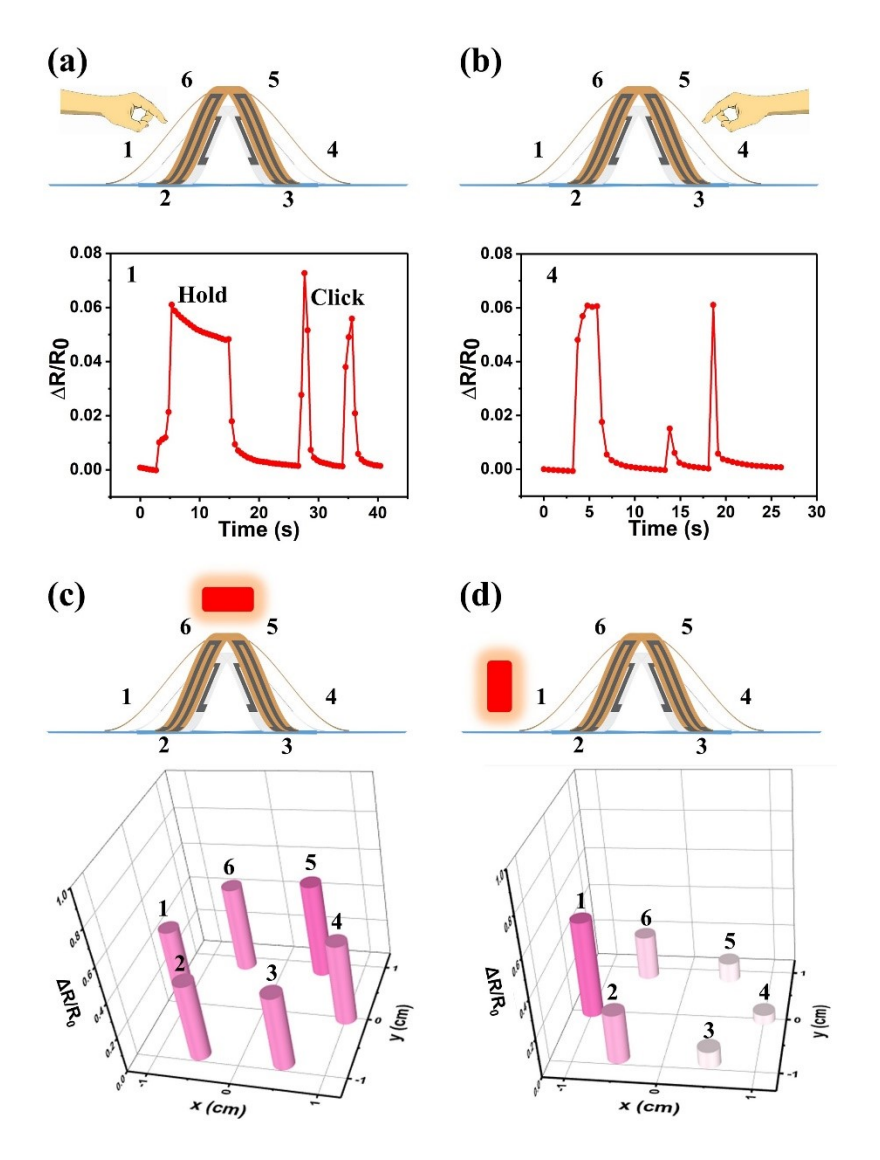


Figure 5. The spatially resolved tactile and temperature sensing performance of the assembled 3D sensing system.

The 3D temperature sensor array also shows capability of sensing spatially distributed temperatures. As shown in Figure 5c, when a heat source (200 °C) was placed 10 cm right above

of the 3D sensor array, which resulted in the same distance to all six individual temperature sensors, the resistances of all the sensors were increased by a similar amplitude of ~ 45%, which corresponded to ~56 °C according to the results shown in Figure 4c. We also used an infrared (IR) camera (FLIR E60) to measure the temperature as shown the Figure S11. The measured result agrees well with the value suggested from the LIG temperature sensors, confirming the accuracy of the LIG-silicone based temperature sensors. [33] If the heat source was moved to the left side with 10 cm away from the sensor of Temp-1, the six temperature sensors exhibited different resistance changes (Figure 5d) due to varied distances to the heat source. The one closer to the heat source showed a larger resistance increase. Through this spatially resolved 3D sensing system, the temperature distribution can be detected in 3D space and the direction of heat source can be approximately derived.

3. CONCLUSIONS

In summary, we have demonstrated a novel assembly of 3D structures for bifunctional sensors. The assembly is driven by thermally responsive hydrogels. Besides the advantages inherited from the mechanically guided buckling method such as wide choice of materials and geometric validity, the resulting 3D structures show responsiveness to the benign stimulus i.e., a moderate temperature, reversibility in 2D-to-3D shape transformation, and high structural complexity. A diversity of complex 3D structures have been assembled as platforms for 3D electronics. The demonstrated 3D bifunctional sensing system has illustrated the functions of spatially resolved tactile and temperature sensing. The proposed strategy would pave a new route to development of 3D electronics for applications in biomedical devices, artificial limbs, robotics, and so forth.

4. EXPERIMENTAL SECTION

Fabrication of PNIPAM hydrogel substrate. The PNIPAM was synthesized according to the previously reported recipe. [41] In details, 300 mg N-isopropylacrylamide (NIPAM) monomer (ACROS Organic) and 30 mg methylene-N,N'-bis(acrylamide) (MBAA) crosslinker (ACROS Organic) were dissolved in 2 mL deionized (DI) water by sonication for 5 min. Then, 11 μL N,N,N',N'-tetramethylethylenediamine (TEMED, purchased from ACROS Organic) were added in the solution as the polymerization accelerator. After 540 μL ammonium peroxodisulfate (APS, purchased from Sigma Aldrich) in 1% aqueous solution was added as initiator, the solution was quickly poured into an aluminum dish. The polymerization started within 3 min and was completed after 1 h. The polymerized hydrogel was immersed into DI water for 24 h to remove the non-polymerized monomers.

The shapes of the hydrogels were patterned by DLW using a Universal laser system (VLS 2.30) with characteristics of 10.6 µm wavelength, 120 µm beam size, 14 µs pulse duration, 30 W maximum power, and 60 cm/s maximum scanning rate. The patterns were first drawn in AutoCAD and then loaded to the laser control software. 100% of the maximum power and 10% of the maximum scanning rate were used to cut the hydrogels. Then the patterned hydrogel was immersed in water at room temperature for hydration.

Fabrication of 2D precursors from SU-8 and polyimide (PI) films. The SU-8 thin films (thickness of 35 μm) were prepared according to the manufacturer protocol (MicroChem). The SU-8 solution (SU-8 2015 series photoresist) was first spin-coated on an aluminum dish (30 s, 3000 rpm) to form a uniform thin film. Then the film was processed by soft baking (95 °C, 3 min), UV exposure (10 mW/cm², 3 min), and post baking (95 °C, 3 min), in sequence. The SU-8 films and PI film (thickness of 25 μm, Kapton) were cut into desired patterns by a CO₂ laser (VLS 2.30).

Fabrication of the LIG-PI strain sensors and LIG-silicone temperature sensors. A laser induction process was employed to carbonize the top layer of the PI films (LIG-PI).^[36-37] The insitu fabricated laser-induced graphene (LIG) and the underneath PI film consists of a LIG-PI strain sensor. To the fabricate temperature sensors, silicone precursor (Dragon Skin series bought from Smooth-on) was first dropped on a LIG-PI film. Then the sample was put in a vacuum oven to make the silicone precursor infiltrate into LIG. After the silicone was cured at room temperature for 4 hours, the LIG-silicone composite film was peeled off. Aluminum electrodes were connected to the sensors by silver paint for electrical measurement.

Measurements. DSC measurement was performed by a Perkin Elmer DSC8500. The temperature program was set in the following way: an isothermal hold at 20 °C for 1 min, a temperature scan from 20 to 45 °C at a scanning rate of 6 °C/min, and an isothermal hold at 45 °C for 1 min. Electrical measurement was conducted by a HP 4156A semiconductor parameter analyzer. A MARK-10 force gauge (model M5-05) was used to measured force.

Finite element analysis (FEA) simulation. FEA simulation was performed in the ABAQUS software. All 2D films were constructed with a deformable shell unit. The elastic modulus and Poisson's ratio were set to 4.02 GPa and 0.22 for SU-8, 40 kPa and 0.15 for the LIG, and 2.5 GPa and 0.34 for the polyimide. For a 3D structure assembled at certain temperature, the corresponding linear shrinkage strain (Figure 2b) was applied to the 2D films in FEA models to simulate the assembly process.

ACKNOWLEDGEMENTS

This work was supported by grants from National Science Foundation (Award number: 1825352) and United States Department of Agriculture (Award number: 2018-67017-27880).

REFERENCES

- [1] B. Tian, J. Liu, T. Dvir, L. Jin, J. H. Tsui, Q. Qing, Z. Suo, R. Langer, D. S. Kohane, C. M. Lieber, *Nat. Mater.* **2012**, *11*, 986.
- [2] T. Ware, D. Simon, K. Hearon, C. Liu, S. Shah, J. Reeder, N. Khodaparast, M. P. Kilgard, D. J. Maitland, R. L. Rennaker, *Macromol. Mater. Eng.* 2012, 297, 1193.
- [3] R. Feiner, L. Engel, S. Fleischer, M. Malki, I. Gal, A. Shapira, Y. Shacham-Diamand, T. Dvir, *Nat. Mater.* **2016**, *15*, 679.
- [4] D. Bishop, F. Pardo, C. Bolle, R. Giles, V. Aksyuk, J. Low Temp. Phys. 2012, 169, 386.
- [5] R. J. Wood, Am. Sci. 2014, 102, 124.
- [6] Z. Yan, F. Zhang, F. Liu, M. Han, D. Ou, Y. Liu, Q. Lin, X. Guo, H. Fu, Z. Xie, Sci. Adv. 2016, 2, e1601014.
- [7] W. Lee, Y. Liu, Y. Lee, B. K. Sharma, S. M. Shinde, S. D. Kim, K. Nan, Z. Yan, M. Han, Y. Huang, *Nat. Commun.* 2018, 9, 1417.
- [8] A. W. Topol, D. La Tulipe, L. Shi, D. J. Frank, K. Bernstein, S. E. Steen, A. Kumar, G. U. Singco, A. M. Young, K. W. Guarini, *IBM J. Res. & Dev.* **2006**, *50*, 491.
- [9] G. Liu, Y. Chen, S. Gao, B. Zhang, R. Li, X. Zhuang, Eng. Sci. 2018, 4, 4.
- [10] C. Shi, H. Qi, R. Ma, Z. Sun, L. Xiao, G. Wei, Z. Huang, S. Liu, J. Li, M. Dong, *Mater. Sci. Eng. C* 2019, 105, 110132.
- [11] H. Gu, H. Zhang, C. Ma, H. Sun, C. Liu, K. Dai, J. Zhang, R. Wei, T. Ding, Z. Guo, J. Mater.
 Chem. C 2019, 7, 2353.
- [12] J.-H. Ahn, H.-S. Kim, K. J. Lee, S. Jeon, S. J. Kang, Y. Sun, R. G. Nuzzo, J. A. Rogers, *Science* **2006**, *314*, 1754.

- [13] P. Benkart, A. Kaiser, A. Munding, M. Bschorr, H.-J. Pfleiderer, E. Kohn, A. Heittmann, H. Huebner, U. Ramacher, *IEEE Des. Test Comput.* **2005**, *22*, 512.
- [14] S. F. Al-Sarawi, D. Abbott, P. D. Franzon, *IEEE Trans. Components Packaging Manufacturing Technol. Part B* **1998**, *21*, 2.
- [15] R. D. Farahani, M. Dubé, D. Therriault, Adv. Mater. 2016, 28, 5794.
- [16] Y. Zhang, F. Zhang, Z. Yan, Q. Ma, X. Li, Y. Huang, J. A. Rogers, *Nat. Rev. Mater.* 2017, 2, 17019.
- [17] J. J. Adams, E. B. Duoss, T. F. Malkowski, M. J. Motala, B. Y. Ahn, R. G. Nuzzo, J. T. Bernhard, J. A. Lewis, *Adv. Mater.* 2011, 23, 1335.
- [18] Y. L. Kong, I. A. Tamargo, H. Kim, B. N. Johnson, M. K. Gupta, T.-W. Koh, H.-A. Chin, D. A. Steingart, B. P. Rand, M. C. McAlpine, *Nano Lett.* 2014, 14, 7017.
- [19] M. S. Mannoor, Z. Jiang, T. James, Y. L. Kong, K. A. Malatesta, W. O. Soboyejo, N. Verma,D. H. Gracias, M. C. McAlpine, *Nano Lett.* 2013, *13*, 2634.
- [20] S. Xu, Z. Yan, K.-I. Jang, W. Huang, H. Fu, J. Kim, Z. Wei, M. Flavin, J. McCracken, R. Wang, *Science* **2015**, *347*, 154.
- [21] J. Wang, Y. Liu, Z. Fan, W. Wang, B. Wang, Z. Guo, *Adv. Compos. Hybrid Mater.* **2019,** *2*, 1.
- [22] J. Reeder, M. Kaltenbrunner, T. Ware, D. Arreaga-Salas, A. Avendano-Bolivar, T. Yokota,
- Y. Inoue, M. Sekino, W. Voit, T. Sekitani, *Adv. Mater.* **2014**, *26*, 4967.
- [23] M. Zarek, M. Layani, I. Cooperstein, E. Sachyani, D. Cohn, S. Magdassi, *Adv. Mater.* **2016**, 28, 4449.
- [24] F. Liu, Y. Chen, H. Song, F. Zhang, Z. Fan, Y. Liu, X. Feng, J. A. Rogers, Y. Huang, Y. Zhang, Small 2019, 15, 1804055.

- [25] Y. Ling, X. Zhuang, Z. Xu, Y. Xie, X. Zhu, Y. Xu, B. Sun, J. Lin, Y. Zhang, Z. Yan, *ACS Nano* **2018**, *12*, 12456.
- [26] Z. Yan, M. Han, Y. Shi, A. Badea, Y. Yang, A. Kulkarni, E. Hanson, M. E. Kandel, X. Wen,F. Zhang, *Proc. Natl. Acad. Sci.* 2017, 114, E9455.
- [27] C. Zhang, J.-W. Su, H. Deng, Y. Xie, Z. Yan, J. Lin, *ACS Appl. Mater. Interfaces* **2017**, *9*, 41505.
- [28] H. Deng, Y. Dong, J.-W. Su, C. Zhang, Y. Xie, C. Zhang, M. R. Maschmann, Y. Lin, J. Lin, *ACS Appl. Mater. Interfaces* **2017**, *9*, 30900.
- [29] H. Deng, C. Zhang, J.-W. Su, Y. Xie, C. Zhang, J. Lin, J. Mater. Chem. B 2018, 6, 5415.
- [30] H. Deng, Y. Dong, C. Zhang, Y. Xie, C. Zhang, J. Lin, Mater. Horizons 2018, 5, 99.
- [31] H. G. Schild, Prog. Polym. Sci. 1992, 17, 163.
- [32] C. Zhang, Y. Xie, H. Deng, T. Tumlin, C. Zhang, J. W. Su, P. Yu, J. Lin, *Small* **2017**, *13*, 1604197.
- [33] B. Sun, R. N. McCay, S. Goswami, Y. Xu, C. Zhang, Y. Ling, J. Lin, Z. Yan, *Adv. Mater.* **2018**, *30*, 1804327.
- [34] M. Heskins, J. E. Guillet, J. Macromol. Sci., Chem. 1968, 2, 1441.
- [35] W. S. Wong, A. Salleo, *Flexible Electronics: Materials and Applications*. Springer Science & Business Media: **2009**; Vol. 11.
- [36] J. Lin, Z. Peng, Y. Liu, F. Ruiz-Zepeda, R. Ye, E. L. Samuel, M. J. Yacaman, B. I. Yakobson, J. M. Tour, *Nat. Commun.* **2014**, *5*, 5714.
- [37] Z. Peng, R. Ye, J. A. Mann, D. Zakhidov, Y. Li, P. R. Smalley, J. Lin, J. M. Tour, *ACS Nano* **2015,** *9*, 5868.
- [38] G. De Maria, C. Natale, S. Pirozzi, Sens. Actuators A-Phys. 2012, 175, 60.

- [39] S. Sundaram, P. Kellnhofer, Y. Li, J.-Y. Zhu, A. Torralba, W. Matusik, *Nature* **2019**, *569*, 698.
- [40] J. Watson, G. Castro, J. Mater. Sci.: Mater. Electron. 2015, 26, 9226.
- [41] C. Yu, Z. Duan, P. Yuan, Y. Li, Y. Su, X. Zhang, Y. Pan, L. L. Dai, R. G. Nuzzo, Y. Huang, *Adv. Mater.* **2013**, *25*, 1541.
- [42] J.-T. Zhang, R. Bhat, K. D. Jandt, Acta Biomater. 2009, 5, 488.
- [43] D. Wirthl, R. Pichler, M. Drack, G. Kettlguber, R. Moser, R. Gerstmayr, F. Hartmann, E. Bradt, R. Kaltseis, C. M. Siket, *Sci. Adv.* **2017**, *3*, e1700053.
- [44] Z. Yan, F. Zhang, J. Wang, F. Liu, X. Guo, K. Nan, Q. Lin, M. Gao, D. Xiao, Y. Shi, *Adv. Funct. Mater.* **2016**, *26*, 2629.
- [45] Z. Yan, M. Han, Y. Yang, K. Nan, H. Luan, Y. Luo, Y. Zhang, Y. Huang, J. A. Rogers, *Extreme Mech. Lett.* **2017**, *11*, 96.
- [46] R. Rahimi, M. Ochoa, W. Yu, B. Ziaie, ACS Appl. Mater. Interfaces 2015, 7, 4463.
- [47] M. Marengo, G. Marinaro, J. Kosel, IEEE Sensors, Glasgow, **2017**, doi: 10.1109/ICSENS.2017.8234429.

Table of Content:

A stimulus responsive assembly method has been developed. The method is capable of assembling various and complex 3D structures from 2D counterparts. Combined with functional materials, these 3D structures have shown spatially resolved functions, including omnidirectional tactile sensing and spatial temperature sensing. These bifunctional 3D sensors would open new applications in soft robotics, bioelectronics, microelectromechanical systems, and so forth.

